BIOCHEMISTRY
including biophysical chemistry & molecular biology

Article

pubs.acs.org/biochemistry

A Novel DNA Binding Mechanism for maf Basic Region-Leucine Zipper Factors Inferred from a MafA−DNA Complex Structure and Binding Specificities

Xun Lu,[†] Gerald P. Guanga,[‡] Cheng Wan,[‡] and Robert B. Rose*[,†]

[†]Department of Molecular and Structural Biochemistry, North Carolina State University, Raleigh, North Carolina 27695, United States

[‡]Z&W Electronics, 500 North Rainbow Boulevard, Suite 300A, Las Vegas, Nevada 89107, United States

Supporting Information

ABSTRACT: MafA is a proto-oncoprotein and is critical for insulin gene expression in pancreatic β-cells. Maf proteins belong to the AP1 superfamily of basic region-leucine zipper (bZIP) transcription factors. Residues in the basic helix and an ancillary N-terminal domain, the Extended Homology Region (EHR), endow maf proteins with unique DNA binding properties: binding a 13 bp consensus site consisting of a core AP1 site (TGACTCA) flanked by TGC sequences and binding DNA stably as monomers. To further characterize maf DNA binding, we determined the structure of a MafA−DNA complex. MafA forms base-specific hydrogen bonds with the flanking $G_{-5}C_{-4}$ and central C_0/G_0 bases, but not with the core-TGA bases. However, in vitro binding studies utilizing a pulse−chase electrophoretic mobility shift assay protocol revealed that mutating either the core-TGA or flanking-TGC bases dramatically increases the binding off rate. Comparing the known maf structures, we propose that DNA binding specificity results from positioning the basic helix through unique phosphate contacts. The EHR does not contact DNA directly but stabilizes DNA binding by contacting the basic helix. Collectively, these results suggest a novel multistep DNA binding process involving a conformational change from contacting the core-TGA to contacting the flanking-TGC bases.

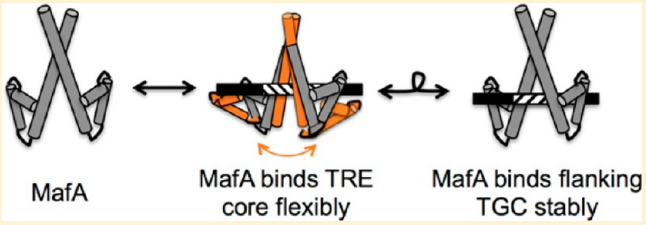

Basic region-leucine zipper (bZIP) proteins constitute one of the largest families of transcription factors in eukaryotes. The dimeric bZIPs perhaps represent the simplest DNA-binding motif, with two long α-helices gripping DNA like a pair of chopsticks.[1] Previous studies of AP1 bZIP proteins have demonstrated that the basic region is unfolded in solution and adopts a helical conformation upon binding to DNA.[2,3] Maf factors are atypical AP1 family members, possessing an Extended Homology Region (EHR) immediately preceding the basic region.[4] The EHR, which is largely helical in solution, facilitates folding of the basic region in the absence of DNA and significantly modifies the binding properties of maf factors.[5,6] Consensus maf-recognition elements (MAREs), TGCTGAC-(G)TCAGCA, contain the canonical TRE or CRE (underlined), typically bound by AP1 factors.[7] According to the type of core, MAREs are named as a TRE-type MARE (T-MARE) or a CRE-type MARE (C-MARE). Recently, an asymmetric maf binding site found in the αA-crystallin promoter was characterized.[8] This site contains an AT-rich sequence 5′ of the MARE half-site that facilitates binding of maf monomers, termed the 5′ATs-half-MARE in this study.

Maf proteins are tissue-specific factors that play key roles in differentiation (reviewed in ref 9). MafA is expressed in pancreatic β-cells and is essential for β-cell maturation and glucose-induced insulin expression.[10−12] L-Maf, the homologue of MafA in chicken, induces lens differentiation.[13] The maf family can be subdivided into two groups. Large mafs, MafA,[14] MafB,[15] c-Maf,[16] and Nrl,[17] contain an N-terminal transactivation domain and function as homodimers or heterodimers with other bZIP partners.[18] Like Fos and Jun, large mafs are proto-oncoproteins and are overexpressed in many human cancers (reviewed in ref 19). Small mafs, MafF,[20] MafG,[21] and MafK,[20] lack an activation domain and act as repressors or rely on dimerization partners for their transcriptional activity (reviewed in ref 22). The crystal structure of MafG bound to a T-MARE variant (TGCTGACTCATCA) has been determined.[6] In this study, we crystallized the bZIP homodimer of the large maf, MafA, bound to the consensus T-MARE, and compared the structure to the known maf structures: the MafG homodimer and the MafB/Fos bZIP heterodimer [Protein Data Bank (PDB) entry 2WT7, no associated article].

The maf structures show that large maf and small maf proteins bind DNA in a similar manner. We found that MafA binds nonspecific DNA with high affinity. Therefore, we developed a pulse−chase electrophoretic mobility shift assay (EMSA) protocol to study off rates from the T-MARE and the 5′ATs-half-MARE. Although the core-TGA was not directly

Received: September 12, 2012
Revised: November 13, 2012
Published: November 13, 2012

contacted by MafA in the structure, it was as crucial as the flanking-TGC for maintaining tight binding. Furthermore, stable DNA binding by a MafA monomer also required the core-TGA and flanking-TGC, aided by the 5′AT-rich sequence. We propose a multistep binding mechanism in which MafA first binds the TRE core like other AP1 bZIP factors. Then a conformational change allows MafA to bind the flanking-TGC as in the crystal structure. Given that authentic maf binding sites are often asymmetric and contain only a half-site of the consensus MARE,[10,13,23,24] monomeric and sequential binding may be biologically relevant.

EXPERIMENTAL PROCEDURES

Plasmid Construction, Protein Expression, and Purification. MafA (residues 226−318) and ΔMafA (residues 226−280) were cloned into a modified pET24b vector, with an N-terminal six-His affinity tag followed by a thrombin cleavage site. To prevent disulfide bond formation, the two cysteine residues in the sequence were mutated to serine (C271S and C287S) by site-directed mutagenesis using Phusion high-fidelity DNA polymerase (Finnzyme). MafA (226−318)_C271S_C287S (hereafter called MafA, unless specified) and ΔMafA (226−280)_C271S (hereafter called ΔMafA) were expressed in *Escherichia coli* BL21(DE3) STAR cells (Invitrogen), grown at 37 °C to an OD_{600} of 0.6, and induced with 1 mM isopropyl β-D-1-thiogalactopyranoside (IPTG) overnight at 22 °C. Proteins were purified by nickel affinity chromatography (Sigma) according to the manufacturer's instructions with a high-salt buffer [800 mM NaCl and 100 mM Tris-HCl (pH 7.8)]. The His tag was cleaved by thrombin (MP Biomedicals) and removed by rebinding to nickel affinity resin. Because there is no tryptophan residue in the protein sequence, the protein concentration was measured by the Bradford assay (Bio-Rad). Amino acid analysis of MafA indicated that the concentrations were overestimated by the Bradford assay by ∼50% [Molecular Structure Facility at the University of California, Davis, CA (data not shown)]. The corrected concentrations were reported.

Preparation and Crystallization of the MafA−MARE Complex. Complementary oligonucleotides containing the consensus T-MARE were purchased from Integrated DNA Technologies, Inc., for crystallization. Oligonucleotides were annealed in an annealing buffer [100 mM NaCl, 1 mM EDTA, and 10 mM Tris-HCl (pH 8.0)] at 95 °C and slowly cooled to room temperature. Crystallization trials were conducted with oligonucleotides 16−22 bp in length with different end configurations. Optimal crystals grew with 19 bp oligonucleotides with Hoogsteen base pair end joining: 5′-CCCTGCTGACTCAGCACCG and 5′-CCGGTGCTGAGTCAGCAGG.[25] Annealed oligonucleotides were mixed with purified MafA (without cysteine mutations) at a 1:4 DNA:protein ratio to ensure that all the oligonucleotides were bound. The MafA−MARE complex was formed during stepwise dialysis to a low salt level: from 800 to 500 to 250 to 150 mM NaCl with 2 mM $MgCl_2$ and 10 mM HEPES (pH 7.8). Excess MafA protein precipitated at low salt concentrations and was removed by centrifugation. The complex was concentrated to 6.7 mg/mL for crystallization. The best crystals grew from sitting drops from a pH gradient by mixing a 1:1 ratio of protein sample and buffer A [1.8 M ammonium sulfate and 100 mM sodium citrate (pH 5.5)] with a different volatile buffer B [1.2 M ammonium sulfate and 100 mM sodium acetate (pH 4.5)] in the reservoir. Crystals grew at 18 °C.

X-ray Data Collection and Structure Determination. Crystals were transferred to a cryoprotectant containing the mother liquor with 20% glycerol and flash-frozen in liquid nitrogen. Data were collected at 100 K, using synchrotron beamline 22ID of the Southeast Regional Collaborative Access Team (SER-CAT) at the Advanced Photon Source (APS, Argonne National Laboratory, Argonne, IL). Data were processed using XDS.[26] Initial phases were derived by molecular replacement using Phaser.[27] The search model was based on the MafG dimer (PDB entry 3A5T) with side chain differences mutated to alanine and the 15 bp DNA.[6] Manual model building was conducted in Coot,[28] and structure refinement utilized Refmac5[29,30] and Phenix.[31] Structures were aligned using LSQMAN[32] for root-mean-square deviation (rmsd) calculations.

Pulse−Chase Electrophoretic Mobility Shift Assay (EMSA). Purified oligonucleotides (Figure 4A) labeled with a near-infrared fluorescent dye, IRDye700 or IRDye800 (Li-COR), were purchased from Integrated DNA Technologies, Inc. Complementary oligonucleotides were annealed as described above. MafA (Figures 4 and 5) or ΔMafA (Figure 6) was incubated for 10 min at 30 °C before being mixed with 6−10 fmol of probes in 20 μL of binding buffer [100 mM KCl, 10 mM HEPES-KOH (pH 7.9), 5 mM $MgCl_2$, 0.1 mM EDTA, 2.5% Tween, 10 mM DTT, 20% glycerol, and 0.5 mg/mL BSA]. Binding reaction mixtures were incubated for 30 min at room temperature, followed by the addition of 2 μL of deionized H_2O or 730 ng/μL poly(dI-dC)-poly(dI-dC). After incubation for an additional 30 min, binding reaction mixtures were loaded onto a prerun polyacrylamide gel (5% unless specified) in running buffer [196 mM glycine, 1 mM EDTA, and 20 mM Tris (pH 8.3)]. Gels were run for 80−150 min at 80 V and 4 °C in the dark to protect the Li-COR dye. Gels were scanned in-plate and analyzed using the Odyssey infrared imaging system (Li-COR).

Small-Angle X-ray Scattering (SAXS). SAXS data were collected on an S-MAX3000 instrument at Rigaku Americas Corp. The MafA−MARE complex was prepared as described for crystallization. Samples were measured at three concentrations (9, 4.5, and 2.25 mg/mL) for 120 min at 4 °C. Sample and buffer images were processed to generate one-dimensional scattering plots using SAXSGUI (Rigaku). Data analysis was performed with Primus.[33] The radius of gyration (R_g) and distance distribution function [$p(r)$] were calculated using GNOM.[34] The calculated scattering profile from the X-ray structure and the comparison with the experimental SAXS data were conducted with Crysol.[35]

RESULTS

Crystallization and Determination of the Structure of the MafA−MARE Complex. The structure of the DNA-binding domain (residues 226−318) of human MafA (NP_963883.2) was determined bound to a 19-mer duplex DNA containing the 13 bp T-MARE consensus sequence and Hoogsteen end-to-end packing of the DNA. Crystals grew reproducibly as the pH was slowly lowered with a volatile buffer, as reported for crystallization of other protein−DNA complexes with Hoogsteen triple-strand DNA end packing.[25] The best crystal diffracted to 2.85 Å resolution. The asymmetric unit contained one MafA dimer bound to a DNA duplex, with a high (75%) solvent content (Matthews coefficient of 4.48). The leucine zipper in the MafA structure was significantly more bent than MafG (Figure 1B); therefore, the 30 C-terminal amino

dx.doi.org/10.1021/bi301248j | *Biochemistry* 2012, 51, 9706−9717

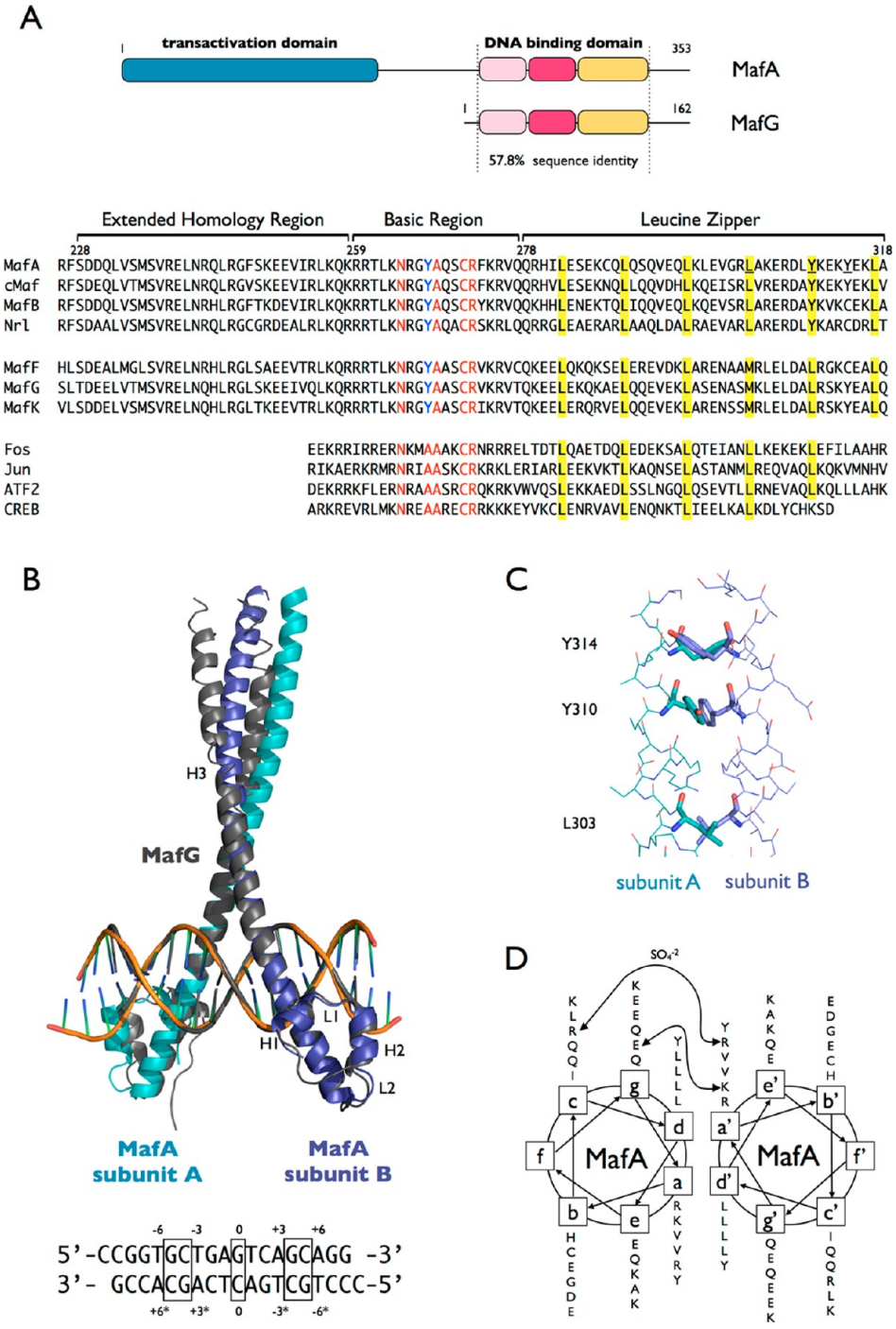

Figure 1. X-ray structure of the MafA–MARE complex. (A) Comparison of the domain structure of a large maf, MafA, and a small maf, MafG: turquoise for the transactivation domain, pink for the extended homology region, red for the basic region, and yellow for the leucine zipper domain. The sequences of the DNA-binding domains of MafA and MafG are 57.8% identical.[55] Protein sequence alignment of large maf (MafA, c-Maf, MafB, and Nrl) and small maf (MafF, MafG, and MafK) factors and other AP1 bZIPs. (B) Superposition of the MafA structure (PDB entry 4EOT, blue and cyan) and the MafG structure (PDB entry 3A5T, black),[6] via alignment of the core DNA sequences (TGACTCA) with an rmsd of 0.410. The basic helices overlap, but the EHRs are rotated relative to each other. Below is shown the DNA sequence in the crystal. The bases contacted through hydrogen bonds in the MafA structure are boxed: central C_0/G_0 and flanking $G_{-5}C_{-4}$. (C) "Tyrosine zipper". Tyr 310 in position "d" and Tyr 314 in position "a" of turns 5 and 6 of the leucine zipper region in the MafA homodimer. (D) Helical-wheel diagram of the leucine zipper region in the MafA homodimer. Arrows represent hydrogen bonds. The hydrogen bond between Arg 302 and Arg 307 is mediated by a SO_4^{2-} ion.

acids were rebuilt manually. The MafA–MARE complex structure was refined to final R and R_{free} values of 0.22 and 0.26, respectively (Table 1).

The consensus 13 bp MARE is pseudopalindromic, with a central C_0/G_0 base pair (Figure 1B). The consensus site is positioned asymmetrically on the 19 bp sequence: three bases from the 5′ end of one strand and four bases from the 5′ end of the other strand. Nevertheless, the orientation of the DNA could not be determined unambiguously from the electron density at this resolution, even after refinement with the DNA

dx.doi.org/10.1021/bi301248j | Biochemistry 2012, 51, 9706–9717

Table 1. Crystallographic Statistics[a]

Data Collection	
space group	$P3_121$
unit cell [*a*, *b*, *c* (Å)]	116.1, 116.1, 85.1
resolution (Å)	20−2.85 (3.00−2.85)
mean $I/\sigma(I)$	22.6 (3.0)
R_{meas} (%)[b]	7.3 (79.8)
completeness (%)	97.5 (85.1)
redundancy	10.8 (9.4)
no. of unique reflections	15399 (1880)
Refinement	
R_{work}, R_{free}	0.22, 0.26
no. of reflections	15288
rmsd	
bond lengths (Å)	0.002
bond angles (deg)	0.696
Ramachandran plot, favored regions (%)	100
B factor (Å^2)	
protein (subunit A, B)	92.0, 91.4
DNA (strand C, D)	89.6, 83.5
solvent	83.9
ligand	119.8

[a]Values in parentheses indicate statistics for the highest-resolution bin. [b]Redundancy-independent *R* factor.[54]

built in either orientation (data not shown). The deposited structure was refined with the DNA oriented in the direction with the lower *R* factor and slightly better fit to the electron density.

Overall Structure of the MafA−MARE Complex. The extended homology region (EHR) and basic region of large maf and small maf proteins are highly conserved (Figure 1A). After the alignment of the 7 bp TRE core DNA sequence in the MafA and MafG structures, the basic helices were positioned identically in the major groove (Cα atoms of residues A254−272 and B254−272 superimposed with an rmsd of 0.6 Å), while the EHRs of MafA were slightly rotated relative to the MafG structure (Figure 1B; Cα atoms of residues A228−253 and B228−253 superimposed with an rmsd of 2.6 Å).[6] The EHR of MafA was identical in structure to MafG (Cα atoms of MafA and MafG residues A228−253 superimposed with an rmsd of 0.8 Å), suggesting some flexibility in the position of this domain.

The leucine zipper sequences of MafA and MafG are less conserved, and large and small maf proteins reportedly do not form heterodimers.[15] The coiled coil in the MafG structure is almost symmetrically positioned relative to the DNA, whereas the coiled coil in MafA is significantly bent (Figure 1B). The bend in the coiled coil of MafA is similar to that of Fos/Jun in complex with NFAT.[36] Given the symmetry of the MafA homodimer, the bending probably results from crystal packing interactions, also observed in other bZIP structures.[37,38] Nevertheless, the curvature of the zipper does not affect the positioning of the basic helices in the major groove of the DNA.

In the MafG structure, dimerization specificity was attributed to three hydrogen bonding interactions in the leucine zipper: a direct hydrogen bond between Gln 82 and Lys 83 (in the "a" and "g" helical-wheel positions), a water-mediated contact between Gln 75 and Lys 76 (in the "a" and "g" positions), and a hydrogen bond between the two Asn 97 residues in the "a" position of the coiled coils.[6] Few interhelical interactions were observed in the MafA homodimer (Figure 1D). A salt bridge between Glu 285 and Lys 286 replaces the Gln 82−Lys 83 interaction of MafG. The importance of this interaction is implied by the K320E (K286 in MafA) mutation of c-Maf, another large maf, in cataract patients.[39] The indirect hydrogen bond between Gln 75 and Lys 76 was not formed by Arg 279 (instead of Lys 76) of MafA. Kurokawa et al. suggested that the interaction between Asn 97 ("a" position) might explain the dimerization selectivity of MafG for small mafs.[6] In MafA, Val at the equivalent position contributes to the hydrophobic core of the homodimer (Figure 1A). In both MafG and MafA, one of the Leu residues in the hydrophobic core, the "d" position of the coiled coil, is modified: in small mafs by methionine at turn 4 and in large mafs by tyrosine at turn 5 (Figure 1A,C). These hydrophobic interactions may contribute to the dimerization selectivity of large and small maf factors.

MafA Contacts the Flanking GC and Central C_0/G_0 Bases. The consensus maf-binding site can be divided into three distinct regions: C_0/G_0 at the center of the TRE core, core-TGA residues adjacent to the C_0/G_0 base pair (numbered ±3 to ±1), and flanking-TGC residues 5′ of the TRE core (numbered ±6 to ±4) (Figure 1B).[7] The basic helices of most bZIP factors primarily contact the core. Like MafG, the basic helices of MafA contact the flanking $G_{-5}C_{-4}$ bases through two conserved residues: Asn 264 (MafG Asn 61) and Arg 260 (MafG Arg 57) (Figure 2A). Asn 264 in MafA contacts C_4 directly (<3.2 Å) in both subunits of MafA instead of an indirect and a weak hydrogen bond (>3.2 Å) in MafG.[6] The only hydrogen bond contacts with the TRE core bases are those of Arg 272 with the central G_0 and C_0 (Figure 2B). The corresponding residues in MafG, Arg 69, contact the central bases indirectly through water in one monomer and the phosphate backbone in the other monomer. The interaction of Arg 272 with the central C_0/G_0 bases is highly conserved in all AP1 factors (PDB entries 1FOS, 2H7H, 1JNM, 2DGC, and 1T2K).[37,40,41] Arg 272 in chain B of MafA adopts two conformations: one conformation, like Arg 272 in chain A, contacting the base and one conformation pointing away from the DNA (Figure 2B). Two conformations of Arg 272 are also observed in higher-resolution AP1 structures such as JUN (PDB entry 2H7H) and GCN4 (PDB entry 2DGC) homodimers. A central ligand, larger than a water molecule or chloride ion, coordinates interactions by Arg 272 and Arg 275 from both MafA subunits (Figure 2B). The electron density was modeled as a sulfate ion, originating from the crystallization solution. There is no sulfate ion in the MafG structure, suggesting that the sulfate ion might stabilize the Arg 272−C_0/G_0 base contacts in MafA.

The phosphate contacts by the basic helices of MafA extend to the flanking-TGC residues (Figure 2C, left), while the phosphate contacts by other AP1 bZIP factors, such as c-Fos, are clustered toward the TRE core (Figure 2C, right).[37] Both MafA monomers contact the phosphate backbone at two sites in the core: Arg 265 NH2 with T_1 O1P and Thr 261 OG1 with C_2 O2P (not formed in MafG). The phosphate contacts by the MafA homodimer are not perfectly symmetric: Gln 269 NE2 contacts C_0 O2P in chain A only, and Lys 274 NZ contacts T_{-3} O1P in chain B only (Figure S1 of the Supporting Information). Two MafA residues form strong hydrogen bonds with phosphates of the flanking bases: Tyr 267 OH with G_{-5} O2P (~2.5 Å) and Arg 259 NH2 with T_{-6} O2P (2.8 and 3.1 Å) (Figure S2 of the Supporting Information). In MafG, Arg 56 (Arg 259 in MafA) contacts only the phosphate backbone of one monomer. Tyr 267 inserts into the major

dx.doi.org/10.1021/bi301248j | *Biochemistry* 2012, 51, 9706−9717

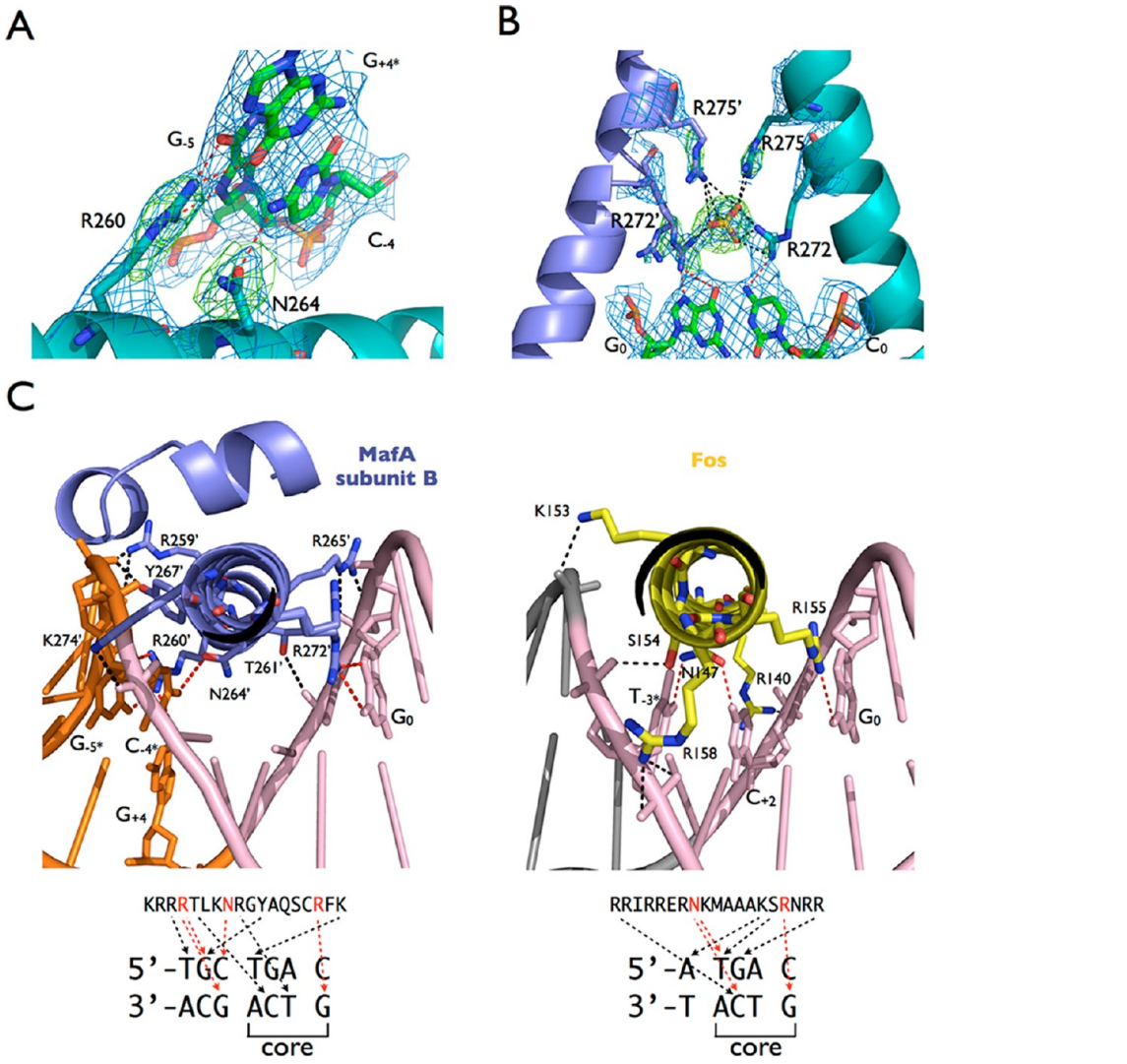

Figure 2. Interactions between MafA and MARE. (A) Arg 260 (NH1 and NH2) and Asn 264 OD1 in subunit A make direct hydrogen bonds with the flanking $G_{-5}C_{-4}$ sequence. Arg 264 also contacts G_4 (O6). The electron density is calculated from a simulated annealing omit map with the Arg 260 and Asn 264 side chains omitted. (B) Sulfate-coordinated Arg 272 in subunits A and B contacts the central C_0/G_0. The electron density is calculated from a simulated annealing omit map with an individual residue (R272 or R272′ or R275 or R275′) or the sulfate ion omitted. Omit maps are contoured at 1σ for $2F_O - F_C$ (dark blue) and at 4σ for $F_O - F_C$ (green for positive, red for negative). (C) MafA basic helix residues primarily contact the flanking $G_{-5}C_{-4}$ bases (left), while Fos basic helix residues primarily contact the AP1 core (right, PDB entry 1FOS).[37] Direct hydrogen bonding interactions (···) with bases are colored red and with the phosphate backbone are colored black. The view is along the basic helix from the N-terminus, contacting the major groove. The TRE core sequence is colored pink in both structures. The protein–DNA interactions are also represented schematically.

groove kinking the DNA backbone (Figure S3C of the Supporting Information). This kinking is observed in only maf structures, and not in other bZIP proteins (PDB entries 1FOS, 1SKN, and 2H7H).[6,37,42] The phosphate contacts by Thr 261 and Tyr 267 are unique to maf proteins.[43]

Comparisons of maf– and Fos–DNA Complexes. As in MafG, the EHR of MafA does not contact the DNA directly. To understand how maf proteins bind DNA differently than canonical AP1 factors, we compared the MafA homodimer–DNA structure with the MafB/Fos heterodimer–DNA structure (PDB entry 2WT7, 2.3 Å resolution, re-refined by PDB_REDO which reported better statistics[44]). The DNA-binding domain sequences of MafA and MafB are almost identical (Figure 1A). Via the alignment of 10 bp of DNA encompassing the TRE core and one MARE half-site (TGCTGACTCA) (rmsd of 0.5 Å), the basic regions of MafA and MafB overlap exactly (Cα rmsd for MafA residues B255–272 and MafB residues B239–256 of 0.46 Å) (Figure S3 of the Supporting Information). On the other hand, the N-terminus of the basic region in c-Fos is slightly tilted (Cα rmsd for MafA residues A255–272 and Fos residues A138–155 of 1.2 Å). The distance between the Arg 143 Cα atom of c-Fos and the corresponding Arg 260 Cα atom of MafA is 1.3 Å, long enough to prevent hydrogen bonding with the base of G_{-5}. Therefore, the position of the basic helix may contribute to maf proteins contacting the flanking-TGC bases instead of the core-TGA bases.

We next compared the *B* factors of MafA, MafB, and c-Fos to evaluate differences in the mobility of the basic domains. The basic helix of MafB is significantly more ordered than the basic helix of c-Fos (Figure 3A). Particularly striking is the difference in mobility of Arg 143 in c-Fos, with an average position

dx.doi.org/10.1021/bi301248j | *Biochemistry* 2012, 51, 9706–9717

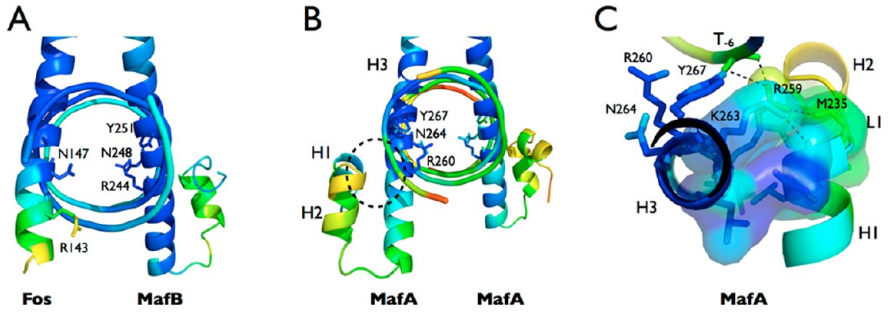

Figure 3. EHR stabilizes the basic helix. The DNA binding domains of MafB/Fos (A, PDB entry 2WT7) and MafA (B and C) are colored according to the overall *B* factor. (A) The basic helix of MafB is well-ordered (blue, *B* factor of 15), while the basic helix of c-Fos is less well ordered than MafB. Arg 143 has a *B* factor of ∼70 (yellow). We propose the high mobility of Arg 143 contributes to its not contacting a base, unlike the equivalent Arg 244 in MafB. The relative *B* factor colors are blue for −15, cyan for −30, green for −45, and yellow for −75. (B) In the MafA homodimer structure, the basic helix is the most stable region of the protein, like MafB in the MafB/Fos structure. The overall *B* factor of this structure (2.85 Å resolution) is higher than the *B* factor of the MafB/Fos structure (2.3 Å resolution). The *B* factor colors from low to high are blue for −55, cyan for −80, green for −100, yellow for −130, and red for −160. The view is along the DNA helical axis. (C) The circled region in panel B is displayed, along the H3 helical axis. Hydrophobic residues in H1, H2, and the basic helix pack tightly. Arg 259 forms a bridge between the EHR (the carbonyl oxygen of Met 235 in L1) and the basic helix (the backbone phosphate of T_{-6}). Dotted lines represent hydrogen bonds.

pointing toward the solvent, and the equivalent Arg 244 in MafB, which has a low temperature factor and contacts two DNA bases (Figures 2A and 3A). The basic helix of MafA is ordered like MafB (Figure 3B). Arg 260 (equivalent to Arg 143 in c-Fos and Arg 244 in MafB) is embedded in the most stable region of MafA. The maf-specific EHR, which extends the basic helix and forms two additional short helices, appears to stabilize the basic helix via hydrogen bonding and van de Waals interactions with the basic region (Figure 3C).

Sequence-Specific Off Rates of MafA−DNA Binding. To confirm the importance of the base contacts in the MafA structure, we performed EMSAs using a series of DNA probes with mutations in the MARE sequence (Figure 4A). A time course with the MARE probe indicated that MafA reached equilibrium in <30 min (Figure S4 of the Supporting Information). The binding affinity (judged by the protein concentration required to bind 50% of the DNA) was ∼0.7 nM as measured by an EMSA without dIdC added (Figure S5 of the Supporting Information). These data did not fit the hyperbolic equation (rmsd = 0.18) but did fit the Hill equation with a K_d of 0.46 nM and an n of 2.9 (rmsd = 0.04). Competition assays with a cold competitor were consistent with low nanomolar binding (Figure 4B). Surprisingly, a nonspecific competitor (mut_MARE) with mutations in bases that are directly contacted by MafA in the crystal structure (positions 0, ±4, and ±5) competed just 3-fold less efficiently than the specific competitor. The high affinity for nonspecific DNA was confirmed with dIdC (Figure S6 of the Supporting Information).

Kerppola et al. reported that maf proteins dissociate slowly from consensus DNA binding sites.[43] Therefore, we compared binding off rates with a pulse−chase EMSA protocol, having excess dIdC compete with the bound DNA probes. A time course in the presence of a high concentration of competitor dIdC demonstrated that mutations in the consensus MARE sequence increased the off rate (Figure S7 of the Supporting Information). To compare the off rates from different DNA sequences, binding reactions were assessed at an arbitrary time of 30 min after the dIdC competitor had been added. MafA bound tightly to the 13 bp MARE, displaying no dissociation after 30 min (Figure 4C). Mutating the central C_0/G_0 base pair (CEN probe) did not affect the off rate, while mutating one copy of the flanking-TGC (TGC probe) sequence dramatically increased the off rate (Figure 4C,D). Surprisingly, mutating the core-TGA sequence also increased the off rate, indicating that these bases are as crucial as the flanking-TGC sequence for tight binding despite the absence of hydrogen bond interactions in the crystal structure (Figure 4E). Yoshida et al. proposed that 5′AT-rich sequences adjacent to the 13 bp MARE increased the binding affinity of MafA.[8] In our study, however, MafA dimers bound MARE and MARE_AT probes with similar affinities and off rates (Figure S8 of the Supporting Information). We also analyzed binding of MafA to the native insulin promoter. The insulin site (INS probe) is asymmetric: one half-site with a 5′AT-rich sequence contains two substitutions in the core-TGA sequence, and the other half-site contains one substitution in the flanking-TGC sequence (Figure 4A). MafA bound the insulin site with an affinity similar to that of the MARE probe, but with a faster off rate (Figure 4F). EMSA results are summarized in Figure 4G.

Stable Binding to 5′AT-Rich Half-MARE Sites. To investigate the importance of the 5′AT-rich sequence for binding asymmetric sites, we measured binding to a 5′ATs-half-MARE (HALF probe) with substitutions in the second half-site.[8] The MafA dimer bound the 5′ATs-half-MARE almost as tightly as the symmetric MARE probe (Figure 5A). The off rate from the insulin site (INS probe, AAAT TGC aGc C) was faster than from the 5′ATs-half-MARE (HALF probe) (compare Figures 4F and 5A), confirming the importance of the core-TGA sequence for half-site binding. Surprisingly, a second shift (S2) was visible on the gel at low MafA concentrations (Figure 5B). S2 was never observed with other probes, including the INS probe. Given that MafA binds DNA as a monomer, we considered that the lower MafA band might be a monomer binding tightly to the 5′AT-half-MARE.[8]

To test the binding of a MafA monomer, we truncated the leucine zipper dimerization domain. The resulting ΔMafA bound the 5′ATs-half-MARE (Figure S9 of the Supporting Information). We then tested binding on the MARE_AT probe, which contains two 5′ATs-half-MARE sites (Figure 6A). As expected, a second ΔMafA bound to the other 5′ATs-half-MARE site in the MARE_AT probe, confirming that ΔMafA bound the 5′ATs-half-MARE as a monomer. Interestingly, some ΔMafA remained bound as a monomer even at 480 nM,

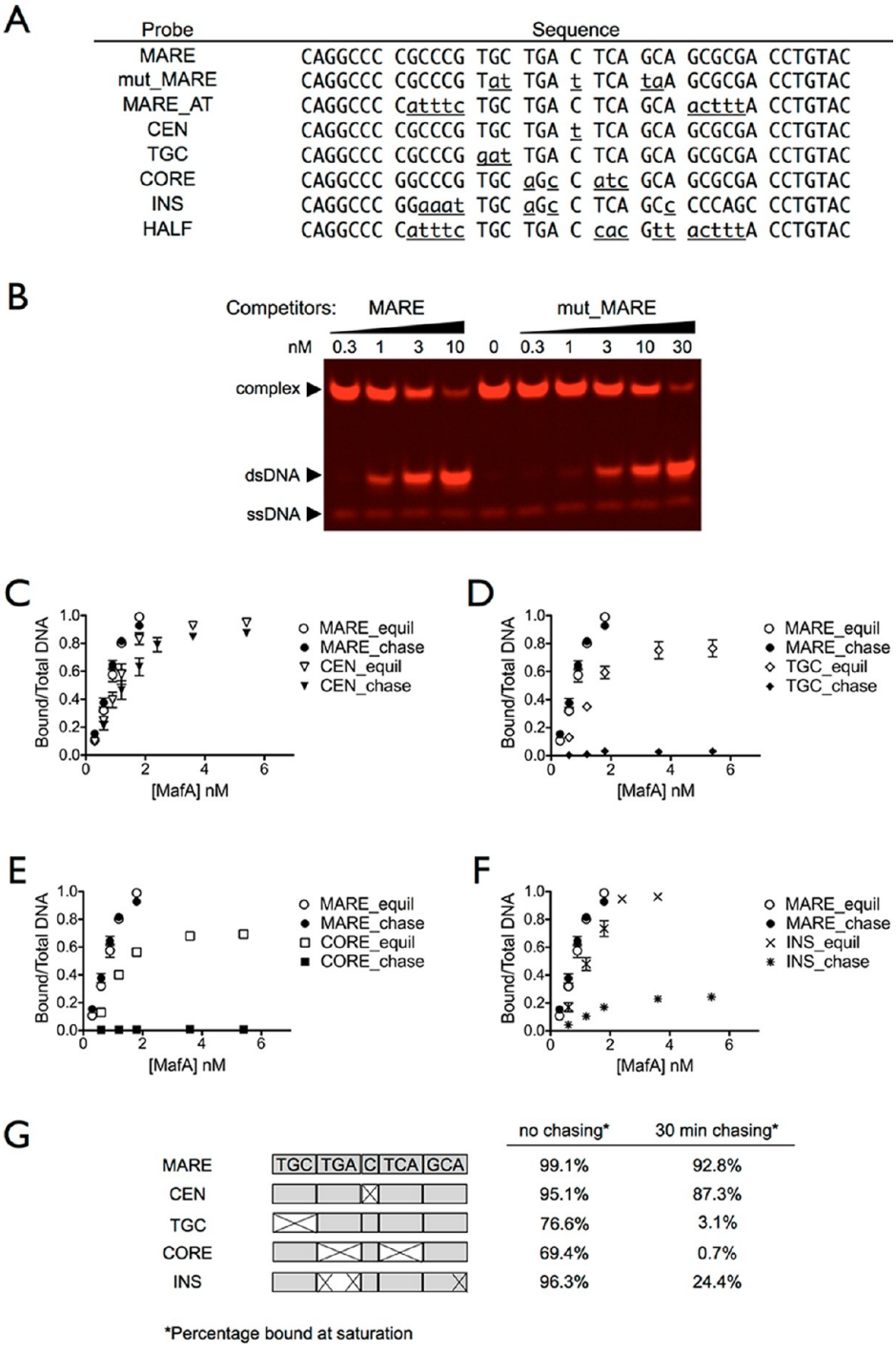

Figure 4. MafA binds consensus and mutated MARE sites with distinct off rates. (A) Sequences of oligonucleotide probes used in EMSAs. Mutations shown with lowercase letters are underlined. (B) EMSA showing 1.8 nM MafA binding to 0.3 nM labeled MARE probe. A nonspecific competitor (mut_MARE) competed just 3-fold less well than the unlabeled MARE. (C−F) Comparison of MafA equilibria in the absence of dIdC (MARE_equil, empty symbols) and off rates (MARE_chase, filled symbols) of the consensus MARE probe with mutations in the (C) central C_0/G_0 (CEN), (D) flanking-TGC (TGC), and (E) core-TGA (CORE) sequences and with the (F) asymmetric INS sequence. All probes bound at equilibrium with a similar affinity (MafA concentration at half-maximal binding), but mutations in the flanking-TGC (D) or core-TGA (E) sequence increased the off rate dramatically, diminishing the final equilibrium binding below saturation. The INS probe (F) showed a moderate off rate. (G) Summary of the DNA binding results. Data were averaged from at least three independent experiments (error bar is the standard error of the mean). Binding assays were conducted with 0.5 nM probe.

suggesting negative cooperativity between monomers. ΔMafA bound the HALF probe with an affinity similar to that of the MafA dimer, but the off rate was faster (Figure 6B). The level of binding of the monomer was significantly reduced without the 5′ATs (MARE probe) or a perfect TRE core (INS probe), but binding was detectable at a high (120 nM) MafA concentration (Figure 6C). When the 5′ATs were absent, further loss of the core-TGA or flanking-TGC sequence abolished the binding completely, but the C_0/G_0 mutation (CEN probe) was tolerated.

dx.doi.org/10.1021/bi301248j | *Biochemistry* 2012, 51, 9706−9717

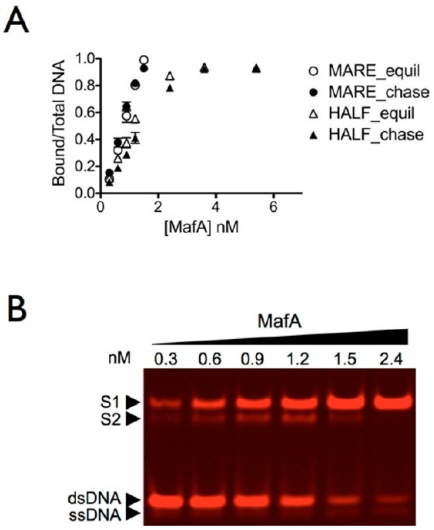

Figure 5. MafA bound the 5′ATs-half-MARE with a slow off rate. (A) Equilibrium assays (empty symbols) and pulse−chase assays (filled symbols) were conducted with 0.3 nM MARE probe or 0.5 nM HALF probe. Data were averaged from at least three independent experiments (error bar is the standard error of the mean). (B) MafA binding to the HALF probe indicated two shifts, S1 and S2. The lower band, S2, was likely a MafA monomer bound to the 5′ATs-half-MARE sequence.

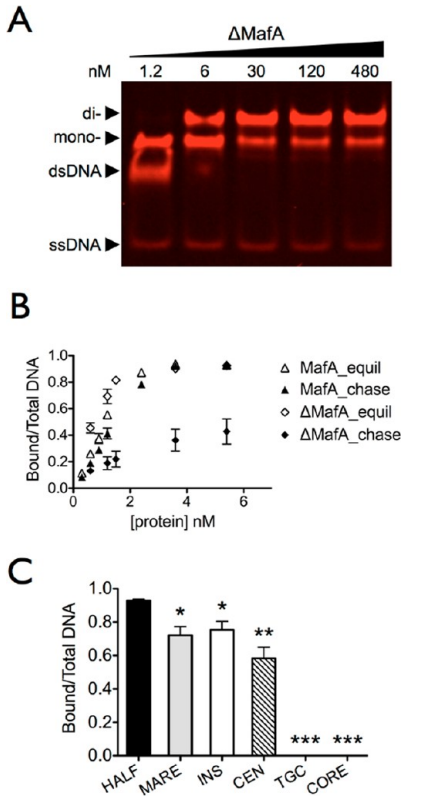

Figure 6. ΔMafA bound DNA as a monomer. (A) One or two ΔMafA monomers bound the MARE_AT probe (0.5 nM), as resolved on an 8% acrylamide gel. (B) ΔMafA bound the HALF probe with high affinity (◇) and moderate off rate (◆). MafA data (△ and ▲, same as in Figure S7 of the Supporting Information) are displayed for comparison. Data were averaged from at least three independent experiments (error bar is the standard error of the mean). (C) ΔMafA (120 nM) bound sequences that lack an intact 5′ATs-half-MARE site with an affinity significantly lower than that for the HALF probe. Three independent experiments were conducted. *t* test against the HALF probe: $*p < 0.05$, $**p < 0.01$, $***p < 0.001$.

Solution Structure of the MafA−MARE Complex Using SAXS. To investigate the solution conformation of the MafA−MARE complex, SAXS data were collected at three concentrations (Figure 7A). The samples were monodispersed according to the Guinier plots and the extrapolated $I(0)$ that varied linearly with sample concentration (Table 2 and Figure 7B). The radius of gyration (R_g) estimated from the Guinier plots and the pair distance distribution functions, $p(r)$, agreed with the R_g calculated from the crystal structure, ∼34 Å, including a 3 Å solvent shell (Figure S10 of the Supporting Information). Finally, the scattering curve calculated from the crystal structure fit the experimental scattering data well (Figure 7B). Therefore, the MafA−MARE complex in solution resembles the dimer in the crystal structure.

DISCUSSION

Maf bZIP domains differ from other AP1 bZIP domains, such as Fos and Jun, because of a conserved N-terminal ancillary DNA binding domain, the Extended Homology Region (EHR), and several unique residues in the basic helix (Thr 261, Gly 266, and Tyr 267).[4−6] These attributes significantly modify the DNA binding properties of maf proteins, binding 13−14 bp MARE sites instead of 7−8 bp TRE/CRE sites.[1,37] In the study presented here, we compared quantitative measurements of DNA binding by MafA monomers and dimers with DNA contacts in a crystal structure bound to a consensus T-MARE sequence. We propose a multistep DNA binding model to explain the discrepancy between binding kinetics and the crystal structure contacts.

MAREs Defined by Off Rates. The consensus MAREs, TGCTGAC(G)TCAGCA, were identified by the selection and amplified binding assay with c-Maf in 1994.[7] Another group associated the maf consensus site with the flanking-TGC bases only.[4] In the study presented here, we measured the binding kinetics of the MafA bZIP domain. The MafA dimer bound to all DNA sequences tested with an affinity (measured as the protein concentration producing half-maximal binding) of ∼1 nM, in the absence of a dIdC competitor (Figure 4). We found that MafA bound nonspecific DNA with high affinity. Other bZIP proteins (Fos, CREB, and ATF) also bind nonspecific DNA with high affinity.[45,46] Nonspecific DNA binding by CREB does not induce ordering of the basic helices, adopting a non-native conformation.[46] Therefore, the affinity of bZIP factors for DNA is not a good measure of specificity. In contrast, the off rate of MafA varies greatly depending on the DNA sequence, as previously described.[43] We compared off rates with a pulse−chase EMSA protocol, allowing the bound MafA to dissociate for 30 min in the presence of excess dIdC. According to off rates, binding of MafA to the consensus T-MARE site depends equally on the core-TGA and flanking-TGC bases and is insensitive to substitutions in the central C_0/G_0 bases (Figure 4). The contribution of the core-TGA sequence to binding was previously shown by surface plasmon resonance.[47]

MafA Binding to Endogenous Asymmetric Half-MAREs. The basic helices of most bZIP factors fold in conjunction with DNA binding.[48] In contrast, the basic helix and the EHR of MafA fold in solution and bind DNA stably as a monomer.[5,8,43] The consensus half-site for monomer binding consists of a TGCTGAC half-MARE with an adjacent 5′AT-

dx.doi.org/10.1021/bi301248j | *Biochemistry* 2012, 51, 9706−9717

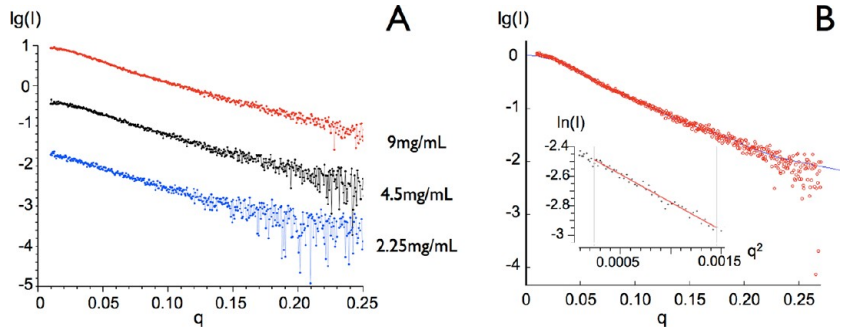

Figure 7. Solution scattering of the MafA–MARE complex agrees with the crystal structure. (A) SAXS profiles of the MafA–MARE complex at three concentrations: 2.25, 4.5, and 9 mg/mL. Curves are translated for display. (B) The scattering curve (blue) calculated from the crystal structure of the MafA–MARE complex fits the observed SAXS data (9 mg/mL); χ^2 = 1.87 (Crysol).[35] The inset shows the Guinier plot.

Table 2. Overall SAXS Parameters of the MafA–MARE Complex

		$p(r)^b$		Crysol	
concn (mg/mL)	Guinier R_g[a] (Å)	R_g (Å)	$I(0)$	χ^2	shell R_g (Å)
9	33.8 ± 0.5	34.0 ± 0.2	0.090	1.87	34.0
4.5	30.7 ± 0.6	32.5 ± 0.3	0.040	1.07	
2.25	33.4 ± 1.3	33.1 ± 0.4	0.018	0.97	

[a] R_g was estimated with qR_g < 1.3. [b] The pair distance distribution function, $p(r)$, was analyzed with a D_{max} of 108 Å (Figure S10 of the Supporting Information).

rich sequence.[8,49] A MafA monomer (ΔMafA), lacking the leucine zipper dimerization domain, bound to the consensus 5′AT-half-MARE with high affinity in the absence of dIdC, but with a measurable off rate (Figure 6B). The 5′AT, flanking-TGC, and core-TGA sequences are all required for tight monomer binding (Figure 6C). Binding of the dimer to the 5′AT-half-MARE decreased the off rate (Figures 5A and 6B). Interestingly, the 5′AT-half-MARE selects for MafA monomer binding even in the presence of MafA homodimers (Figure 5B), either binding MafA monomers present in solution or dissociating a MafA monomer of the dimer from the nonspecific half-site. Stable binding of maf monomers may facilitate formation of heterodimers on promoter sites, which are generally asymmetric.[8,10,11,13] The insulin MafA binding site is asymmetric with a MARE half-site that diverges from the consensus 5′AT-half-MARE, increasing the off rate of MafA homodimers (Figure 4F). Both MafA homodimers and MafA/ATF2 heterodimers can bind and activate insulin gene expression.[18,50] The physiological role of MafA heterodimers in β-cells is unknown.

MafA Structure. The MafA homodimer structure confirms that large maf proteins, which include an N-terminal activation domain, bind the consensus T-MARE sequence the same as small maf proteins.[6,51] Like conventional bZIP proteins, all direct base contacts by the Maf bZIP domain are mediated through the basic helix; the EHR does not contact DNA directly.[6] As previously noted, the residues contacting the flanking $G_{-5}C_{-4}$ bases (MafA Asn 264 and Arg 260) are not unique to maf proteins, but the orientation of these residues is unique, eliminating the contacts with the core-TGA sequence (Figure 2C and Figure S3B of the Supporting Information). The interpretation proposed from the MafG structure focused on positioning the Asn 264 and Arg 260 side chains through a hydrogen bonding network and water-mediated contacts unique to maf domains, among Tyr 64, Arg 57, and Asn 61 (MafA Tyr 267, Arg 260, and Asn 264).[6] In addition, the Maf-specific Thr 58 (MafA Thr 261) was proposed to disrupt an Arg 57 (MafA Arg 260)–phosphate contact, also contributing to orienting Arg 57 toward the flanking-TGC sequence.

In contrast with the MafG structure, in the MafA structure the hydrogen bonding network with Asn 264 and Arg 260 is not apparent. While this may be a limitation of a low-resolution structure, we propose an alternate explanation based on global positioning of the basic helix and thermal stability due to EHR contacts. We compared the MafA homodimer structure with the MafB/Fos heterodimer structure (PDB entry 2WT7) by superimposing the 10 bp DNA, including the TRE core and one flanking-TGC. The position of the basic helix in the major groove was identical for the MafA and MafB monomers but differed for the MafA monomer and Fos (Figure S3 of the Supporting Information). Different phosphate backbone contacts situate the basic helices: in MafA, Thr 261 contacts a phosphate in the core, and Arg 259 and Tyr 267 contact phosphates in the flanking region. The phosphate contacts by Fos are primarily within the core. The difference in the position of the basic helix is sufficient to shift Arg 143 (MafA Arg 260) by 1.3 Å, precluding interaction with a DNA base (Figure S3 of the Supporting Information). In addition, the EHR stabilizes the basic helix through hydrophobic contacts (Figure 3C) and hydrogen bonds by Arg 259 from the basic helix with the EHR (Met 136 carbonyl) and the DNA phosphate backbone (T_{-6} O1P). Deleting the EHR significantly impairs DNA binding.[4,6] In contrast, the basic helix of Fos is mobile, as reflected by high B factors (Figure 3A).

Multistep Binding Models for MafA on Symmetric and Asymmetric MAREs. DNA binding by MafA does not fit hyperbolic kinetics but fits a Hill equation with a Hill coefficient of >2 (Figure S5 of the Supporting Information). Positive cooperativity might result from MafA dimerization on the DNA or conformational changes upon MafA binding. Moreover, the flanking-TGC and core-TGA mutations yield binding curves that never reached saturation at high MafA concentrations, indicative of a multistep binding profile (Figure 4D–F and Figure S11 of the Supporting Information). The crystal structure depicts a MafA homodimer bound to the consensus T-MARE in a single conformation with direct hydrogen bonds to the flanking-TGC bases (Figure 2C).[6] To explain the dependence of maf binding on the core-TGA sequence, we propose that MafA binds a specific MARE site in at least two steps (Figure 8A). In step 1, initially the basic helix contacts the core bases and backbone phosphates like Fos/Jun. During this step, binding is unstable because of high thermal motion, and

dx.doi.org/10.1021/bi301248j | Biochemistry 2012, 51, 9706–9717

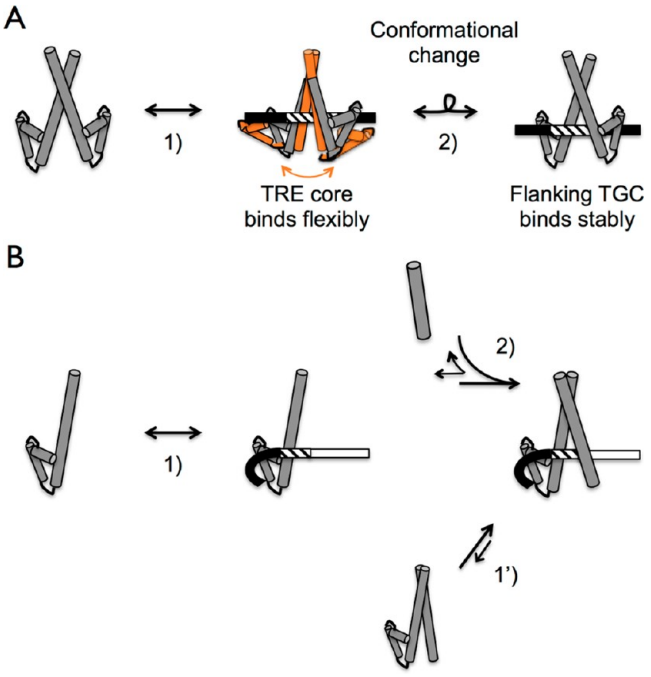

Figure 8. Multistep models for MafA–DNA binding. (A) For the symmetric MARE, (1) MafA binds as a dimer. Initially the basic helices contact the TRE core-TGA bases like other bZIP factors and the position of the basic helices in the major grooves is flexible (orange arrow). (2) After a conformational change by side chains contacting the phosphate backbone and the EHR, the basic helices become locked in a state binding to the flanking-TGC. (B) For the asymmetric 5'ATs-half-MARE, (1) MafA binds as a monomer, (2) followed by binding of a second bZip monomer. (1') Alternatively, MafA binds as a homo- or heterodimer. The 5'AT-rich sequence (curved black bar) is depicted to bend and interact with basic residues on the surface of the EHR. However, no structural information for the binding of MafA to the 5'AT-rich sequence is available. The bound dimer has a slow off rate (1' and 2 off rates). A conformational change may be required as for the dimer model, because the flanking-TGC and core-TGA bases both contribute to monomer binding. The black bar represents 5'AT-rich and flanking-TGC sequences, the striped bar core-TGA sequences, and the white bar non-specific DNA sequence.

the position of the EHR is flexible (Figure 3). In step 2, the EHR is properly positioned to stabilize the contacts with the flanking-TGC bases and backbone phosphates (Figure 3C). The slow step in positioning the EHR might include inserting Tyr 267 in the major groove and the associated kink in the DNA backbone (Figures S2A and S3C of the Supporting Information) and inserting Arg 259 between the EHR and DNA phosphate backbone (Figure 3C and Figure S2B of the Supporting Information).

Binding to a 5′ATs-half-MARE also utilizes the core-TGA and flanking-TGC bases, but the mechanism is distinct, as demonstrated by the dependence on a 5′AT-rich sequence and stable binding of a monomer (Figure 6). How the 5′AT-rich sequence facilitates monomer binding is not clear. One possibility is that the intrinsic curvature of the 5′AT tract facilitates DNA bending, allowing phosphate contacts with basic residues on the EHR surface, by Arg 238, Arg 242, Arg 245, and Lys 249 (all but Arg 242 are conserved among maf sequences) (Figure 1A). Studies of Fos/Jun identified basic residues (KRR) N-terminal of the basic helix of Fos that facilitate DNA bending, enhanced by AT sequences flanking the core DNA sequence.[45,52] DNA bending toward the minor groove due to interactions with the 5′AT-rich sequence may explain the negative cooperativity for binding two MafA monomers to adjacent MARE_AT sites (Figure 6A).[53]

We propose MafA binds to asymmetric promoter sites in multiple steps (Figure 8B). Stable binding of MafA monomers (step 1) facilitates binding of heterodimer partners (step 2). The dependence of MafA monomer binding on the core-TGA sequence may result from a similar conformational change described for homodimer binding. Once the dimer forms, it locks MafA in place with a very slow off rate (Figure 6B).

CONCLUSIONS

Our structure demonstrates that large and small maf proteins bind DNA similarly. Nonspecific DNA binding by the Maf bZIP domain indicates that the off rate is a better measure of specificity than affinity. Maf bZIP domains are unique among bZIP factors in their ability to bind DNA stably as a monomer. We envision that stable binding by MafA monomers enhances heterodimer formation on authentic asymmetric promoter sites. We propose that MafA binds DNA through a novel multistep mechanism involving a conformational change from interactions with the TRE core, like other bZIP factors, to interactions with the flanking-TGC bases captured in the crystal structures. Future mutagenesis and kinetic studies will test the role of this conformational change in maf DNA binding. The kinetics of maf DNA binding will determine how maf enhancer sites are regulated.

ASSOCIATED CONTENT

Supporting Information

Figures with details of results from crystal structure analysis, EMSAs, and SAXS. This material is available free of charge via the Internet at http://pubs.acs.org.

Accession Codes

Atomic coordinates and X-ray data have been deposited into the RCSB Protein Data Bank as entry 4EOT.

AUTHOR INFORMATION

Corresponding Author

*Telephone: (919) 513-4191. E-mail: bob_rose@ncsu.edu.

Funding

This work was supported by National Science Foundation Grant MCB-0643830.

Notes

The authors declare no competing financial interest.

ACKNOWLEDGMENTS

We thank Michael S. German, M.D., for the human MafA construct. We are also grateful to Drs. Jianhua Li and Mark Del Campo at Rigaku Americas Corp. for SAXS data collection, processing, and analysis. Data were collected at Southeast Regional Collaborative Access Team (SER-CAT) beamline 22-ID at the Advanced Photon Source. Supporting institutions may be found at http://www.ser-cat.org/members.html.

ABBREVIATIONS

MafA, v-maf musculoaponeurotic fibrosarcoma oncogene homologue A; bZIP, basic region-leucine zipper; EHR, extended homology region; MARE, maf-recognition element; EMSA, electrophoretic mobility shift assay; SAXS, small-angle X-ray scattering; TRE, TPA-response element; CRE, cAMP-response element.

REFERENCES

(1) Ellenberger, T. E., Brandl, C. J., Struhl, K., and Harrison, S. C. (1992) The Gcn4 Basic Region Leucine Zipper Binds DNA as a Dimer of Uninterrupted α-Helices: Crystal-Structure of the Protein-DNA Complex. *Cell 71*, 1223−1237.

(2) Patel, L., Abate, C., and Curran, T. (1990) Altered protein conformation on DNA binding by Fos and Jun. *Nature 347*, 572−575.

(3) Weiss, M. A., Ellenberger, T., Wobbe, C. R., Lee, J. P., Harrison, S. C., and Struhl, K. (1990) Folding transition in the DNA-binding domain of GCN4 on specific binding to DNA. *Nature 347*, 575−578.

(4) Kerppola, T. K., and Curran, T. (1994) A Conserved Region Adjacent to the Basic Domain Is Required for Recognition of an Extended DNA-Binding Site by Maf/Nrl Family Proteins. *Oncogene 9*, 3149−3158.

(5) Kusunoki, H., Motohashi, H., Katsuoka, F., Morohashi, A., Yamamoto, M., and Tanaka, T. (2002) Solution structure of the DNA-binding domain of MafG. *Nat. Struct. Biol. 9*, 252−256.

(6) Kurokawa, H., Motohashi, H., Sueno, S., Kimura, M., Takagawa, H., Kanno, Y., Yamamoto, M., and Tanaka, T. (2009) Structural Basis of Alternative DNA Recognition by Maf Transcription Factors. *Mol. Cell. Biol. 29*, 6232−6244.

(7) Kataoka, K., Noda, M., and Nishizawa, M. (1994) Maf nuclear oncoprotein recognizes sequences related to an AP-1 site and forms heterodimers with both Fos and Jun. *Mol. Cell. Biol. 14*, 700−712.

(8) Yoshida, T., Ohkumo, T., Ishibashi, S., and Yasuda, K. (2005) The 5 ′-AT-rich half-site of Maf recognition element: A functional target for bZIP transcription factor Maf. *Nucleic Acids Res. 33*, 3465−3478.

(9) Blank, V., and Andrews, N. C. (1997) The Maf transcription factors: Regulators of differentiation. *Trends Biochem. Sci. 22*, 437−441.

(10) Olbrot, M., Rud, J., Moss, L. G., and Sharma, A. (2002) Identification of β-cell-specific insulin gene transcription factor RIPE3b1 as mammalian MafA. *Proc. Natl. Acad. Sci. U.S.A. 99*, 6737−6742.

(11) Kataoka, K., Han, S. I., Shioda, S., Hirai, M., Nishizawa, M., and Handa, H. (2002) MafA is a glucose-regulated and pancreatic β-cell-specific transcriptional activator for the insulin gene. *J. Biol. Chem. 277*, 49903−49910.

(12) Matsuoka, T. A., Artner, I., Henderson, E., Means, A., Sander, M., and Stein, R. (2004) The MafA transcription factor appears to be responsible for tissue-specific expression of insulin. *Proc. Natl. Acad. Sci. U.S.A. 101*, 2930−2933.

(13) Ogino, H., and Yasuda, K. (1998) Induction of lens differentiation by activation of a bZIP transcription factor, L-maf. *Science 280*, 115−118.

(14) Benkhelifa, S., Provot, S., Lecoq, O., Pouponnot, C., Calothy, G., and Felder-Schmittbuhl, M. P. (1998) mafA, a novel member of the maf proto-oncogene family, displays developmental regulation and mitogenic capacity in avian neuroretina cells. *Oncogene 17*, 247−254.

(15) Kataoka, K., Fujiwara, K. T., Noda, M., and Nishizawa, M. (1994) MafB, a new Maf family transcription activator that can associate with Maf and Fos but not with Jun. *Mol. Cell. Biol. 14*, 7581−7591.

(16) Kataoka, K., Nishizawa, M., and Kawai, S. (1993) Structure-function analysis of the maf oncogene product, a member of the b-Zip protein family. *J. Virol. 67*, 2133−2141.

(17) Swaroop, A., Xu, J. Z., Pawar, H., Jackson, A., Skolnick, C., and Agarwal, N. (1992) A conserved retina-specific gene encodes a basic motif/leucine zipper domain. *Proc. Natl. Acad. Sci. U.S.A. 89*, 266−270.

(18) Han, S. I., Yasuda, K., and Kataoka, K. (2011) ATF2 Interacts with β-Cell-enriched Transcription Factors, MafA, Pdx1, and Beta2, and Activates Insulin Gene Transcription. *J. Biol. Chem. 286*, 10449−10456.

(19) Eychene, A., Rocques, N., and Pouponnot, C. (2008) A new MAFia in cancer. *Nat. Rev. Cancer 8*, 683−693.

(20) Fujiwara, K. T., Kataoka, K., and Nishizawa, M. (1993) Two new members of the maf oncogene family, mafK and mafF, encode nuclear b-Zip proteins lacking putative trans-activator domain. *Oncogene 8*, 2371−2380.

(21) Kataoka, K., Igarashi, K., Itoh, K., Fujiwara, K. T., Noda, M., Yamamoto, M., and Nishizawa, M. (1995) Small Maf proteins heterodimerize with Fos and may act as competitive repressors of the NF-E2 transcription factor. *Mol. Cell. Biol. 15*, 2180−2190.

(22) Motohashi, H., Shavit, J. A., Igarashi, K., Yamamoto, M., and Engel, J. D. (1997) The world according to Maf. *Nucleic Acids Res. 25*, 2953−2959.

(23) Gosmain, Y., Avril, I., Mamin, A., and Philippe, J. (2007) Pax-6 and c-Maf functionally interact with the α-cell-specific DNA element G1 in vivo to promote glucagon gene expression. *J. Biol. Chem. 282*, 35024−35034.

(24) Cao, S. J., Liu, J. G., Song, L. H., and Ma, X. J. (2005) The protooncogene c-Maf is an essential transcription factor for IL-10 gene expression in macrophages. *J. Immunol. 174*, 3484−3492.

(25) Tan, S., Hunziker, Y., Pellegrini, L., and Richmond, T. J. (2000) Crystallization of the yeast MATα2/MCM1/DNA ternary complex: General methods and principles for protein/DNA cocrystallization. *J. Mol. Biol. 297*, 947−959.

(26) Kabsch, W. (2010) Xds. *Acta Crystallogr. D66*, 125−132.

(27) McCoy, A. J., Grosse-Kunstleve, R. W., Adams, P. D., Winn, M. D., Storoni, L. C., and Read, R. J. (2007) Phaser crystallographic software. *J. Appl. Crystallogr. 40*, 658−674.

(28) Emsley, P., Lohkamp, B., Scott, W. G., and Cowtan, K. (2010) Features and development of Coot. *Acta Crystallogr. D66*, 486−501.

(29) Vagin, A. A., Steiner, R. A., Lebedev, A. A., Potterton, L., McNicholas, S., Long, F., and Murshudov, G. N. (2004) REFMAC5 dictionary: Organization of prior chemical knowledge and guidelines for its use. *Acta Crystallogr. D60*, 2184−2195.

(30) Bailey, S. (1994) The Ccp4 Suite: Programs for Protein Crystallography. *Acta Crystallogr. D50*, 760−763.

(31) Adams, P. D., Afonine, P. V., Bunkóczi, G., Chen, V. B., Davis, I. W., Echols, N., Headd, J. J., Hung, L.-W., Kapral, G. J., Grosse-Kunstleve, R. W., McCoy, A. J., Moriarty, N. W., Oeffner, R., Read, R. J., Richardson, D. C., Richardson, J. S., Terwilliger, T. C., and Zwart, P. H. (2010) PHENIX: A comprehensive Python-based system for macromolecular structure solution. *Acta Crystallogr. D66*, 213−221.

(32) Kleywegt, G. J. (1996) Use of non-crystallographic symmetry in protein structure refinement. *Acta Crystallogr. D52*, 842−857.

(33) Konarev, P. V., Volkov, V. V., Sokolova, A. V., Koch, M. H. J., and Svergun, D. I. (2003) PRIMUS: A Windows PC-based system for small-angle scattering data analysis. *Appl. Crystallogr. 36*, 1277−1283.

(34) Svergun, D. I. (1992) Determination of the regularization parameter in indirect-transform methods using perceptual criteria. *J. Appl. Crystallogr. 25*, 495−503.

(35) Svergun, D., Barberato, C., and Koch, M. H. J. (1995) CRYSOL: A program to evaluate X-ray solution scattering of biological macromolecules from atomic coordinates. *J. Appl. Crystallogr. 28*, 768−783.

(36) Chen, L., Glover, J. N., Hogan, P. G., Rao, A., and Harrison, S. C. (1998) Structure of the DNA-binding domains from NFAT, Fos and Jun bound specifically to DNA. *Nature 392*, 42−48.

(37) Glover, J. N. M., and Harrison, S. C. (1995) Crystal-Structure of the Heterodimeric Bzip Transcription Factor C-Fos-C-Jun Bound to DNA. *Nature 373*, 257−261.

(38) Fujii, Y., Shimizu, T., Toda, T., Yanagida, M., and Hakoshima, T. (2000) Structural basis for the diversity of DNA recognition by bZIP transcription factors. *Nat. Struct. Biol. 7*, 889−893.

(39) Hansen, L., Mikkelsen, A., Nurnberg, P., Nurnberg, G., Anjum, I., Eiberg, H., and Rosenberg, T. (2009) Comprehensive Mutational Screening in a Cohort of Danish Families with Hereditary Congenital Cataract. *Invest. Ophthalmol. Visual Sci. 50*, 3291−3303.

(40) Keller, W., Konig, P., and Richmond, T. J. (1995) Crystal structure of a bZIP/DNA complex at 2.2 Å: Determinants of DNA specific recognition. *J. Mol. Biol. 254*, 657−667.

(41) Panne, D., Maniatis, T., and Harrison, S. C. (2004) Crystal structure of ATF-2/c-Jun and IRF-3 bound to the interferon-β enhancer. *EMBO J. 23*, 4384−4393.

(42) Rupert, P. B., Daughdrill, G. W., Bowerman, B., and Matthews, B. W. (1998) A new DNA-binding motif in the Skn-1 binding domain DNA complex. *Nat. Struct. Biol. 5*, 484−491.
(43) Dlakic, M., Grinberg, A. V., Leonard, D. A., and Kerppola, T. K. (2001) DNA sequence-dependent folding determines the divergence in binding specificities between Maf and other bZIP proteins. *EMBO J. 20*, 828−840.
(44) Joosten, R. P., Joosten, K., Murshudov, G. N., and Perrakis, A. (2012) PDB_REDO: Constructive validation, more than just looking for errors. *Acta Crystallogr. D68*, 484−496.
(45) Leonard, D. A., Rajaram, N., and Kerppola, T. K. (1997) Structural basis of DNA bending and oriented heterodimer binding by the basic leucine zipper domains of Fos and Jun. *Proc. Natl. Acad. Sci. U.S.A. 94*, 4913−4918.
(46) Metallo, S. J., Paolella, D. N., and Schepartz, A. (1997) The role of a basic amino acid cluster in target site selection and non-specific binding of bZIP peptides to DNA. *Nucleic Acids Res. 25*, 2967−2972.
(47) Yamamoto, T., Kyo, M., Kamiya, T., Tanaka, T., Engel, J. D., Motohashi, H., and Yamamoto, M. (2006) Predictive base substitution rules that determine the binding and transcriptional specificity of Maf recognition elements. *Genes Cells 11*, 575−591.
(48) Miller, M. (2009) The Importance of Being Flexible: The Case of Basic Region Leucine Zipper Transcriptional Regulators. *Curr. Protein Pept. Sci. 10*, 244−269.
(49) Seldeen, K. L., McDonald, C. B., Deegan, B. J., Bhat, V., and Farooq, A. (2010) Dissecting the role of leucine zippers in the binding of bZIP domains of Jun transcription factor to DNA. *Biochem. Biophys. Res. Commun. 394*, 1030−1035.
(50) Zhao, L., Guo, M., Matsuoka, T. A., Hagman, D. K., Parazzoli, S. D., Poitout, V., and Stein, R. (2005) The islet β cell-enriched MafA activator is a key regulator of insulin gene transcription. *J. Biol. Chem. 280*, 11887−11894.
(51) Hang, Y., and Stein, R. (2011) MafA and MafB activity in pancreatic β cells. *Trends Endocrinol. Metab. 22*, 364−373.
(52) Kerppola, T. K., and Curran, T. (1991) DNA Bending by Fos and Jun: The Flexible Hinge Model. *Science 254*, 1210−1214.
(53) Shatzky-Schwartz, M., Arbuckle, N. D., Eisenstein, M., Rabinovich, D., Bareket-Samish, A., Haran, T. E., Luisi, B. F., and Shakked, Z. (1997) X-ray and solution studies of DNA oligomers and implications for the structural basis of A-tract-dependent curvature. *J. Mol. Biol. 267*, 595−623.
(54) Diederichs, K., and Karplus, P. A. (1997) Improved R-factors for diffraction data analysis in macromolecular crystallography. *Nat. Struct. Biol. 4*, 269−275.
(55) Huang, X. Q., and Miller, W. (1991) A Time-Efficient, Linear-Space Local Similarity Algorithm. *Advances in Applied Mathematics 12*, 337−357.